Draft version August 10, 2022
Preprint typeset using LaTeX style AASTeX6 v. 1.0



# TIME-RESOLVED POLARIZATIONS OF GAMMA-RAY BURST PROMPT EMISSION WITH OBSERVED ENERGY SPECTRA

Rui-Rui Wu[1], Qing-Wen Tang[2], and Mi-Xiang Lan[1]
[1]Center for Theoretical Physics and College of Physics, Jilin University, Changchun, 130012, China; lanmixiang@jlu.edu.cn
[2]Department of Physics, School of Physics and Materials Science, Nanchang University, Nanchang 330031, China

## ABSTRACT

Time-resolved polarizations carry more physical information about the source of gamma-ray bursts (GRBs) than the time-integrated ones. Therefore, they give more strict constrains on the models of GRB prompt phase. Both time-resolved and time-integrated polarizations are considered here. The model we use is the synchrotron emission in a large-scale ordered aligned magnetic field. Time-resolved polarizations of GRB prompt phase are derived with the corresponding time-resolved energy spectra. We found the time-integrated PDs calculated with two methods are similar. So it is convenient to estimate the time-integrated PD by the time-integrated energy spectrum. Most of the time-resolved PDs calculated in this paper will increase with time. The trend could match the observed time-resolved PD curve of GRB 170114A, but contrary to the predictions of a decaying PD of both the magnetized internal shock and magnetic reconnection models. PAs calculated in this paper, in general, are roughly constants with time. The predicted PAs here can not match with the violent PA changes observed in GRB 100826A and GRB 170114A. Therefore, more accurate time-resolved polarization observations are needed to test models and to diagnose the true physical process of GRB prompt phase.

*Keywords:* Gamma-ray bursts (629); magnetic fields (994);

## 1. INTRODUCTION

The origins of the cosmological gamma-ray bursts (GRBs) remain mysterious. Although the light curves show rich diversities, both the time-integrated and time-resolved energy spectra of these violent explosions can be typically described by an empirical Band function (Band et al. 1993). Band function is a smoothly connected broken power law, with high- and low-energy spectral indices $\beta$ and $\alpha$ linked at peak energy $E_p$. Polarization is determined by the asymmetry of the system. In GRBs, such asymmetry can originate from the magnetic field (Sari 1999; Granot & Königl 2003; Toma et al. 2009; Lan et al. 2019), jet structure (Rossi et al. 2004; Wu et al. 2005; Lan et al. 2018), and observational geometry (Waxman 2003). Toma et al. (2009) had considered the time-integrated polarizations of GRB prompt phase with large-scale toroidal magnetic field. They used the energy spectra, i.e., the Band function, to construct the time-integrated Stokes parameters.

Time-integrated polarization observations of GRB prompt phase show rich diversities. The observed polarization degrees (PDs) are around 10% for POLAR's detection (Zhang et al. 2019; Kole et al. 2020), while they are concentrated above 50% for AstroSat's measurements (Chattopadhyay et al. 2019; Chand et al. 2019; Gupta et al. 2022). Guan & Lan (2022) had interpreted the time-integrated observational data of GRB prompt phase using the observed time-integrated energy spectra. They found polarizations of synchrotron emission in a large-scale ordered magnetic field could match most of the data from the Gamma-ray Burst Polarimeter (GAP) and POLAR, while the observed data of the AstroSat were obviously higher than the theoretical predicted values of the same model.

Time-integrated polarizations, compared with the time-resolved ones, have erased lots of evolution information about the source. For example, it is possible to diagnose the reasons for the observed lower time-integrated PD values than the theoretically predicted ones (Guan & Lan 2022). There are a few time-resolved polarization observations in GRB prompt phase so far (Yonetoku et al. 2011; Zhang et al. 2019; Burgess et al. 2019). The abrupt 90 degree Polarization angle (PA) change can happen either between two pulses in GRB 100826A (Yonetoku et al. 2011) or between the two time bins within one pulse in GRB 170114A (Zhang et al. 2019). Burgess et al. (2019) had reanalyzed the data of GRB 170114A and divided the prompt phase into 9

time bins. They found, even with large errors, PD of the burst increases and PA rotates with the observational time.

Of the three popular models in GRB prompt phase, the emission mechanisms of the internal shock and the magnetic reconnection models are both the synchrotron emission. The internal shock model involves low- or no-magnetized shells with different velocities and these shells collide with each other, leading to the formation of the internal shocks (Paczynski & Xu 1994; Rees & Meszaros 1994; Fan et al. 2004). If the colliding shells are highly magnetized and the collisions will result in the avalanches of the magnetic reconnection precesses (Zhang & Yan 2011). Time-resolved polarization predictions of both the magnetized internal shock and the magnetic reconnection models were considered recently (Lan et al. 2021; Lan & Dai 2020), and a decaying PD with time is predicted for the two models.

In this paper, time-resolved polarizations of twenty GRBs simultaneously detected by *Fermi* and polarization detectors (i.e., GAP, POLAR, and AstroSat) are calculated based on our time-resolved spectral parameters. We described the model and our numerical results in Section 2. GRB 170114A with time-resolved polarization observation was analyzed in detail in Section 3. The time-integrated PDs of these twenty GRBs were calculated with two methods in Section 4. Our conclusions and discussion were presented in Section 5.

## 2. THE MODEL AND THE NUMERICAL RESULTS

Because the typical time-resolved energy spectra of GRB prompt phases can also be described by the Band function (Band et al. 1993) as the time-integrated ones, we can construct time-resolved Stokes parameters with such Band spectra. Here, as in Guan & Lan (2022), we set the Lorentz factor and the jet half-opening angle of all the bursts to be $\gamma = 100$ and $\theta_j = 0.1$ rad. The redshifts of the bursts are assumed to be 1 if there are no redshift reports (see a collection in Guan & Lan (2022) and references there-in). The magnetic field, in which the accelerated electrons radiate the synchrotron emission, is assumed to be large-scale aligned and its direction is set to be $\delta = \pi/6$.

Of thirty GRBs analyzed in Guan & Lan (2022), twenty are simultaneously detected by *Fermi*. We analyze the public data of *Fermi* to get the parameters of the time-resolved energy spectra of these twenty GRBs. Our data processing are as follows. The rmfit software package in version 432 is employed to perform the spectral analysis. Observational data sets are downloaded in the official web site of *Fermi* Gamma-ray Burst Monitor (GBM) data [1]. We select two NaI detectors (8 keV to 1000 keV) and one BGO detector (200 keV to 40 MeV), both of which are most close to the GRB center position. The ground time-tagged events (TTE) in these three detectors with 2 $\mu$s precision are used in the data reduction. We select one interval before and one after the burst as the background intervals, then employ a polynomial model with one order to fit the background. After that, we thus perform the time-averaged and time-resolved spectral fitting using the chi square statistics. For the time-resolved spectrum, the GBM $T_{90}$ interval in the 50-300 keV energy band is selected as presented in the latest Fermi GBM catalog (von Kienlin et al. 2020). For the time-resolved spectral fitting, we derive the time-resolved time bins by setting a signal to noise ratio between 12 and 100 for individual GRB. A typical Band function is employed in all spectra (Band et al. 1993). All spectral parameters and photon flux of individual spectrum are calculated in the energy band between 8 keV and 40 MeV.

Then the time-resolved Stokes parameters are calculated with these time-resolved spectral parameters. The integrated energy ranges of the Stokes parameters for GRBs with polarization detected by GAP, POLAR, and AstroSat are $50-300$, $50-500$, and $10-100$ keV, respectively. With these time-resolved energy-integrated Stokes parameters, we get the final time-resolved PDs and PAs for each GRB. We have selected five GRBs of total twenty as representatives to analyze their polarization evolutions in details. The results of other fifteen GRBs are presented in Appendix A.

For the polarization model used here (Toma et al. 2009; Guan & Lan 2022), the final energy-integrated polarizations are determined by its spectral parameters ($E_p$, $\alpha$, and $\beta$) and the observational angle ($\theta_V$). The spectral indices ($\tilde{\alpha}$) are positively correlated with the local PD $\pi_0$ [2], hence are positively correlated with the final energy-integrated PD. The spectral index of the low-energy photons ($\alpha$) is usually smaller than that of the high-energy photons ($\beta$). So the local PD $\pi_0$ is smaller for low-energy photons compared with the high-energy photons. The contributions from the low-energy photons with a lower local PD $\pi_0$ will be higher for a spectrum with a larger $E_p$. Therefore, a larger $E_p$ will lead to a lower energy-integrated PD. PD and $E_p$ are negatively correlated.

Because PD is positively corrected with the spectral indices and negatively correlated with the peak energy $E_p$. In our calculation, same as in Guan & Lan (2022),

[1] https://heasarc.gsfc.nasa.gov/W3Browse/fermi/fermigbrst.html

[2] $\pi_0 = (\tilde{\alpha}+1)/(\tilde{\alpha}+5/3)$, $\tilde{\alpha} = \alpha$ for the low-energy photons below $E_p$ and $\tilde{\alpha} = \beta$ for the high-energy photons above $E_p$.

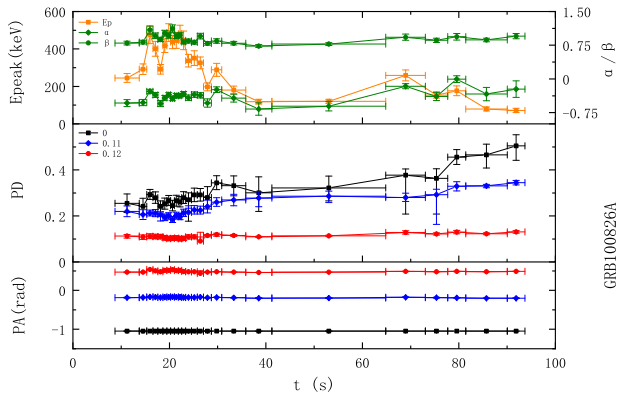


**Figure 1**. Evolutions of the spectral parameters (upper panel), PDs (middle panel), and PAs (lower panel) of GRB 100826A. In the upper panel, the orange squares show the $E_p$s, the green diamonds and circles represent the low- and high-energy spectral index. In the middle and lower panels, the black squares, blue diamonds, and red circles corresponds to 0, 0.11 ($\theta_j + 1/\gamma$), and 0.12 ($\theta_j + 2/\gamma$) rads of the observational angle, respectively.

we use the upper limit of the spectral indices and the lower limit of $E_p$ to derive the upper limit of the PD and PA. The lower limit of the spectral indices and the upper limit of $E_p$ are used to calculate the lower limit of the PD and PA. And the typical values of spectral indices and $E_p$ are used to derive the typical values of the PD and PA.

The $E_p$ evolution pattern is intensity-tracking mode for GRB 100826A. In Fig. 1, PDs increase with observational time $t$ for both on-axis and off-axis observations. PD shows a negative correlation with the peak energy $E_p$. When $E_p$ increases, the contribution from the low-energy part with lower local PD also increase, then the energy-integrated PDs will decrease. PAs stay roughly constants with time for various observational angles. So the model can not produce the violent 90° PA change between two pulses (0-50 and 50-100 s) observed in GRB 100826A (Yonetoku et al. 2011).

The $E_p$ evolution pattern is hard-to-soft mode, meanwhile the low- and high-energy spectral indices are positively correlated for GRB 160802A as shown in Fig. 2. The general trends of PD curves are determined by $E_p$ (i.e., PD increases with a decaying $E_p$.). There are small spikes in the PD curves at early stage, which follow the evolutions of the spectral indices. If the spectral index $\tilde{\alpha}$ increases, local PD $\pi_0$ will increase, then the energy-integrated PD will also increase and vice versa. The polarization of GRB 160802A was detected by Astrosat with a detection energy range of 10-100 keV. At early stage, the time-resolved $E_p$ are all larger than the upper limit of the energy range of the polarization detector. So the energy-integrated Stokes parameters detected by

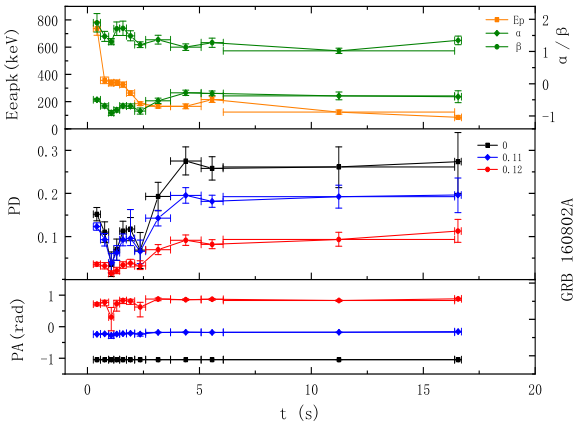


**Figure 2**. Same as Fig. 1, but for GRB 160802A.

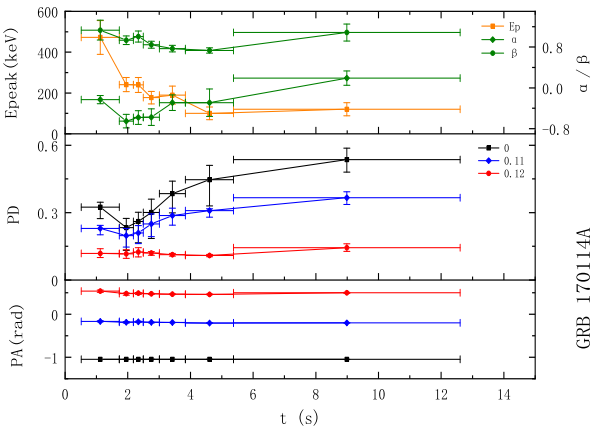


**Figure 3**. Same as Fig. 1, but for GRB 170114A.

AstroSat are completely from the low-energy photons below $E_p$. Therefore, PDs are positively correlated with the low-energy spectral index $\alpha$ at early stage.

Fig. 3 shows the polarization evolution of GRB 170114A with a hard-to-soft mode of $E_p$. At early stage, PDs are obviously positively correlated with the spectral indices for $\theta_V = 0$ and $\theta_V = \theta_j + 1/\gamma$. The evolution of PD is not obvious for $\theta_V = \theta_j + 2/\gamma$. At late stage, $E_p$ decreases and spectral indices increase, resulting in increasing PDs for all three observational angles. PAs of the burst stay roughly constants for various observational angles. Therefore, the polarization model here can not predict the observed PA evolution of the burst, but can reproduce the observed increasing PD curve (Burgess et al. 2019). We have analyzed the polarization evolutions of this burst in details in Section 3.

$\alpha$, $\beta$, and $E_p$ in GRB 160325A show co-evolution as presented in Fig. 4. In the early stage, the evolutions of

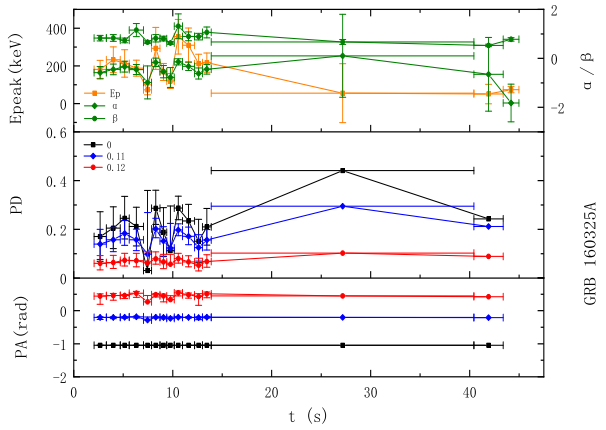


**Figure 4**. Same as Fig. 1, but for GRB 160325A.

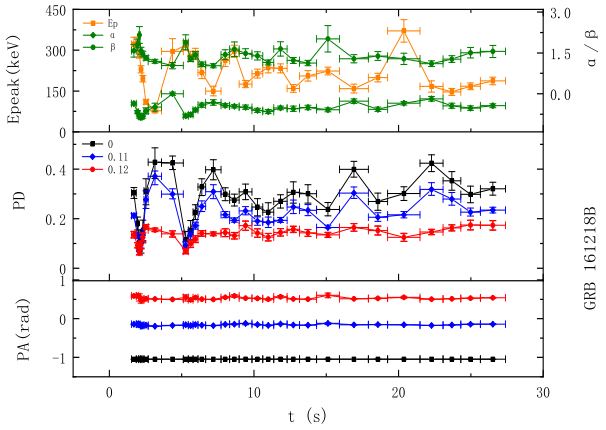


**Figure 5**. Same as Fig. 1, but for GRB 161218B.

PDs track the trends of the spectral indices and $E_p$ for all calculated observational angles. Because the changes of $E_p$ is small at the beginning, their influences on the PD values are very tiny. The evolution trends of PD curves are mainly determined by the spectral indices. The polarization properties of the last point can not be obtained because the upper limit of the low-energy spectral index of this point is still smaller than $-1$ [3].

Fig. 5 shows the polarization evolutions for GRB 161218B. In general, the evolutions of PDs show negative correlations with peak energy $E_p$s. The variation range of $E_p$ is relatively large compared with GRB 160325A shown in Fig. 4 and the evolutions of PDs are mainly determined by $E_p$. At the beginning, $E_p$s are about 350 keV, close to the upper limit 500 keV of POLAR and change shallowly. The main contribution to the Stokes parameters come from low-energy photons. So polarization properties are mainly determined by the spectral index $\alpha$ of the low-energy photons. Therefore, PD curves are positively correlated with the low-energy spectral index at early stage.

## 3. INTERPRETING THE TIME-RESOLVED POLARIZATION DATA OF GRB 170114A

The polarization data of this burst are taken from Burgess et al. (2019). Two sets of the time-resolved spectra are considered here. One set is obtained by analyzing the *Fermi* data, the other is also taken from Burgess et al. (2019). We use both spectra of the burst to calculate its time-resolved polarizations. Our results are shown in Fig. 6. The observational angles of the two fits are $\theta_V = \theta_j + 1/\gamma = 0.11$ rad. The values and trends of the two fits are similar, and both fits the observed PD data equally well.

Because polarization direction keeps unchanged with a variation of $n\pi$ in PA (n is an integer.), here we set the observed PAs in the range of $[-\pi/2, \pi/2]$ by adding or subtracting $n\pi$ from the values given in Burgess et al. (2019). A roughly $-\pi/2$ PA change happens between the second and third points, and a roughly $\pi/2$ PA change happens between the fifth and sixth points. The model used in this paper only predicts a roughly constant PA and can not reproduce such violent PA variations.

Because the minimum time-resolved PD of our best fit is above 20%, which is still larger than the observed time-integrated 4% (Zhang et al. 2019) or 10% (Kole et al. 2020) PD. And the predicted PA of the burst is roughly constant. So the predicted time-integrated PD will be larger than 20%, which is also inconsistent with the observations. For this burst, the observed low time-integrated PD, compared with the high time-resolved PDs, may mainly because of the twice abrupt 90° PA changes. Therefore, more detailed model should be considered to reproduce the observed PA evolution of GRB 170114A.

## 4. TIME-INTEGRATED PDS OF TWENTY BURSTS

Since most of the observed polarization properties of GRB prompt emission are time-integrated values, the time-integrated polarizations can be derived from time-resolved ones. Here, we summarize the time-resolved Stokes parameters to get the time-integrated Stokes parameters. Then the time-integrated polarization properties for the twenty bursts (with both time-resolved spectra obtained from *Fermi* data and polarization observations) can be obtained. We compare these results with both the time-integrated polarizations obtained by the time-integrated spectral parameters and the observed

[3] If the spectral index $\tilde{\alpha}$ is smaller than $-1$, the local PD $\pi_0$ will be smaller than 0.

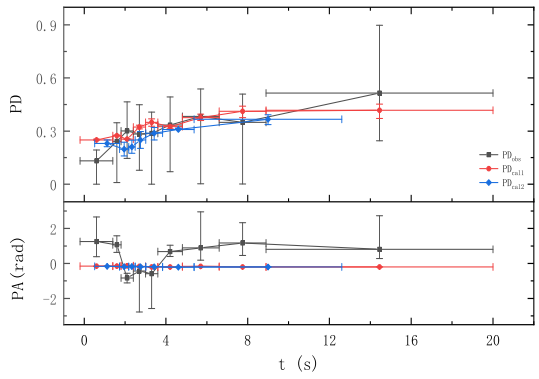


**Figure 6**. Time-resolved polarization of GRB 170114A. The black squares are the observational points, the red circles are calculated with the spectral parameters given in Burgess et al. (2019), and the blue diamonds represent the calculated values using the energy spectra analyzed in this paper. The observational angles of the two fits are $\theta_j + 1/\gamma = 0.11$ rad.

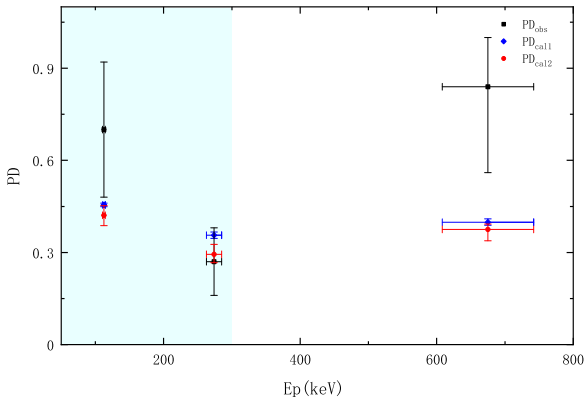


**Figure 7**. Time-integrated PDs of three GRBs detected by GAP. The black squares are the observational values, the red circles are the calculated values using the time-resolved spectra, and the blue diamonds represent the calculated values with the time-integrated spectra. The blue shadow region shows the energy range (50-300 keV) of the GAP.

values.

The time-integrated spectra used here are obtained from analyzing the public data of *Fermi* and are slightly different from that used in Guan & Lan (2022). Time-integrated polarizations of the twenty GRBs are recalculated with both the time-resolved and time-integrated spectra reanalyzed in this paper. The results are shown separately in Figs. 7-9 for GRBs with polarizations detected by GAP, POLAR, and AstroSat, respectively. The calculated time-integrated PDs with two different methods mentioned above of the same burst are similar. Therefore, the time-integrated PD of the single burst can be estimated by the time-integrated energy spectrum.

For three GRBs detected by GAP (Yonetoku et al. 2011, 2012), two of them have the observed PDs larger than the theoretical ones. Because the energy spectra used here and in Guan & Lan (2022) are slightly different, the predicted PDs are slightly smaller than the observed one for GRB 110301A in this paper, but it matches the observed value in Guan & Lan (2022). Nine GRBs of which detected by AstroSat, except for the three upper limits observations, the calculated PDs of the other six GRBs are all smaller than the observed values, in accordance with the results of Guan & Lan (2022).

For POLAR's detections, there are three (GRB 161218B, GRB 170114A, and GRB 170207A) of total eight bursts here with the calculated PDs larger than the observed values. In Guan & Lan (2022), four bursts detected by POLAR with predicted PDs larger than the observed values are GRB 170101A, GRB 170127C,

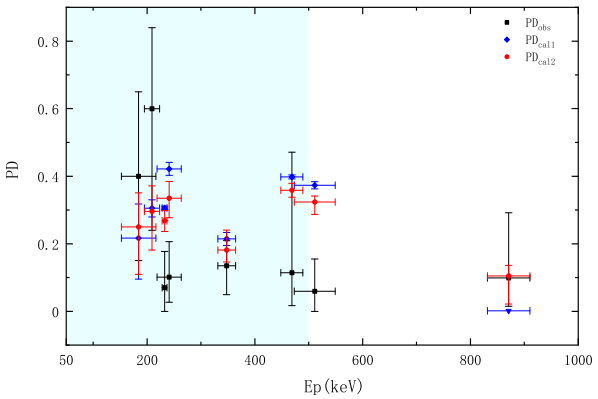


**Figure 8**. Same as Fig. 7, but for GRBs detected by POLAR with detection energy range of 50-500 keV.

GRB 170114A, and GRB 170207A. So two bursts (GRB 170114A and GRB 170207A) have the predicted PDs larger than the observed values for calculations with different spectral parameters, while for GRB 161218B, GRB 170101A, and GRB 170127C, calculations with different spectral parameters will lead to different but consistent results (i.e., consistent with the predictions of the synchrotron-emission model). The spectral parameters used in polarization calculations will affect the final results. The accurate measurements of the spectral parameters are very important for polarization calculations.

## 5. CONCLUSIONS AND DISCUSSION

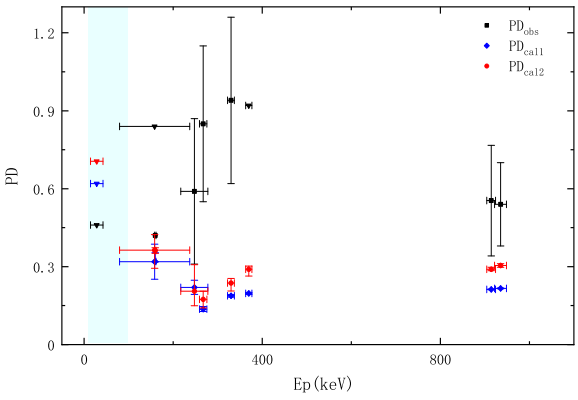


**Figure 9**. Same as Fig. 7, but for GRBs detected by AstroSat in energy range of 10-100 keV.

In this paper, we mainly discuss the time-resolved polarizations of GRB prompt phases with the corresponding time-resolved energy spectra. Then the time-integrated polarizations could be studied by these time-resolved ones. And the obtained time-integrated polarizations are compared with the ones calculated with the time-integrated energy spectra. The main advantage of the model used in this paper (Toma et al. 2009; Guan & Lan 2022) is that it considers the evolutions of the spectral parameters exactly, while the main drawback is that the equal arrival time surface (EATS) effect is not included, so the evolutions of the physical quantities with the radius from the central engine can not be considered.

Time-integrated PDs are similar for the two calculation methods used in this paper, so it is convenient to estimate the time-integrated PDs with the time-integrated energy spectra. The spectral parameters are essential for the calculated PDs. The time-integrated spectral parameters used here are different from that we use in Guan & Lan (2022). For example, the predicted PD here of GRB 161218B detected by POLAR are larger than the observed values, while it matches the observed one in Guan & Lan (2022). Therefore, the accurate observations of the energy spectra are very important. The PDs predicted here are the upper limit because the large-scale ordered aligned magnetic field is assumed in the emitting region. If the observed PDs are larger than the predicted values, the polarization model will be challenged. The conclusions for the time-integrated polarization here are the same as in Guan & Lan (2022). The polarization observations of the AstroSat challenge the synchrotron-emission model, while they are consistent with the synchrotron-emission model in a large-scale ordered magnetic field for POLAR's detections.

If the source is axisymmetric, the Stokes parameters U will be zero and PA of such system can only keep as a constant or change abruptly by 90°. For example, the conical jet with a toroidal magnetic field is such a system. To obtain a gradual evolution of PA, the axial symmetry should be broken. Large-scale ordered aligned magnetic field can offer such asymmetry. Although the magnetic field is assumed to be large-scale aligned, the polarization model here can only predict roughly constant PAs and can not reproduce a large-amplitude evolving PA as observed in GRB 100826A (Yonetoku et al. 2011) and GRB 170114A (Burgess et al. 2019). More detailed models considering the evolutions of the emitting source should be considered.

The calculated PDs are positively correlated with the spectral indices and are negatively correlated with the peak energy $E_p$. Most of the PD curves calculated in this paper will increase with time. The trend could match with that of the only burst (GRB 170114A) having time-resolved polarization observation (Burgess et al. 2019). An increasing PD with time is contrary to the predictions of the magnetized internal shock (Lan et al. 2021) and the magnetic reconnection models (Lan & Dai 2020). The main reason for the difference originates from whether or not the EATS effect is consider. In both the magnetic internal shock and the magnetic reconnection models, the EATS effect is consider and a decaying PD with time is mainly due to the decrease of the $\tilde{f}$ parameter [4] (Lan & Dai 2020). While an increased PD with time is mainly because of a decreased $E_p$ in the model here, in which the EATS effect is not considered. It is amazing that the PD observations of GRB 170114A could be roughly matched with the model prediction in this paper. Therefore, to test models and to determining the physical process of the emitting sources, more and more accurate time-resolved polarization observations are needed.

This paper is dedicated to the 70th anniversary of the physics of Jilin University. This work is supported by the National Natural Science Foundation of China (grant Nos. 11903014, 11903017, 12065017).

[4] $\tilde{f}$ is defined to be the flux ratio between the contributions within and outside the local $1/\gamma$ cone.

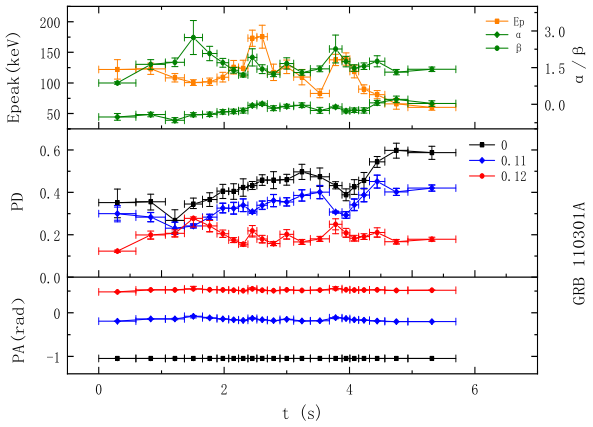


**Figure A1**. Evolutions of the spectral parameters (upper panel), PDs (middle panel), and PAs (lower panel) of GRB 110301A. In the upper panel, the orange squares show the $E_p$s, the green diamonds and circles represent the low- and high-energy spectral index. In the middle and lower panels, the black squares, blue diamonds, and red circles corresponds to 0, 0.11 ($\theta_j + 1/\gamma$), and 0.12 ($\theta_j + 2/\gamma$) rads of the observational angle, respectively.

## REFERENCES


Band, D., Matteson, J., Ford, L., et al. 1993, ApJ, 413, 281

Burgess, J. M., Kole, M., Berlato, F., et al. 2019, A&A, 627, A105

Chand, V., Chattopadhyay, T., Oganesyan, G., et al. 2019, ApJ, 874, 70

Chattopadhyay, T., Vadawale, S. V., Aarthy, E., et al. 2019, ApJ, 884, 123

Fan, Y. Z., Wei, D. M., & Zhang, B. 2004, MNRAS, 354, 1031

Granot, J., & Königl, A. 2003, ApJL, 594, L83

Guan, R. Y., & Lan, M. X. 2022, arXiv e-prints, arXiv:2208.03668

Gupta, R., Gupta, S., Chattopadhyay, T., et al. 2022, MNRAS, 511, 1694

Kole, M., De Angelis, N., Berlato, F., et al. 2020, A&A, 644, A124

Lan, M.-X., & Dai, Z.-G. 2020, ApJ, 892, 141

Lan, M.-X., Geng, J.-J., Wu, X.-F., & Dai, Z.-G. 2019, ApJ, 870, 96

Lan, M.-X., Wang, H.-B., Xu, S., Liu, S., & Wu, X.-F. 2021, ApJ, 909, 184

Lan, M.-X., Wu, X.-F., & Dai, Z.-G. 2018, ApJ, 860, 44

Paczynski, B., & Xu, G. 1994, ApJ, 427, 708

Rees, M. J., & Meszaros, P. 1994, ApJL, 430, L93

Rossi, E. M., Lazzati, D., Salmonson, J. D., & Ghisellini, G. 2004, MNRAS, 354, 86

Sari, R. 1999, ApJL, 524, L43

Toma, K., Sakamoto, T., Zhang, B., et al. 2009, ApJ, 698, 1042

von Kienlin, A., Meegan, C. A., Paciesas, W. S., et al. 2020, ApJ, 893, 46

Waxman, E. 2003, Nature, 423, 388

Wu, X. F., Dai, Z. G., Huang, Y. F., & Lu, T. 2005, MNRAS, 357, 1197

Yonetoku, D., Murakami, T., Gunji, S., et al. 2011, ApJL, 743, L30

—. 2012, ApJL, 758, L1

Zhang, B., & Yan, H. 2011, ApJ, 726, 90

Zhang, S.-N., Kole, M., Bao, T.-W., et al. 2019, Nature Astronomy, 3, 258


## APPENDIX

### A. OTHER 15 GRBS WITH TIME-RESOLVED SPECTRA AND POLARIZATION OBSERVATIONS

For the third points of GRB 160623A, the typical value and lower limit of the low-energy spectral index are both smaller than $-1$, leading to a negative local PD $\pi_0$. And the lower limit of $E_p$ is smaller than 0, which is unphysical. So we can not predict the polarization property of this point. For the second and fourth points of GRB 170127C, the upper limit of the low-energy spectral index $\alpha$ of the two points are both smaller than $-1$. Therefore, the polarizations of the two points can not be derived.

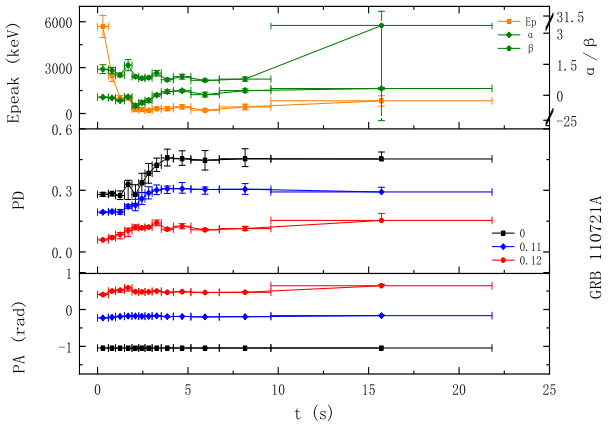


**Figure A2**. Same as Fig. A.1, but for GRB 110721A.

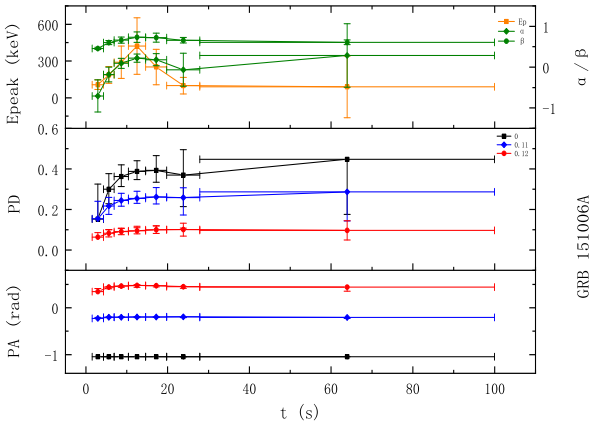


**Figure A3**. Same as Fig. A.1, but for GRB 151006A.

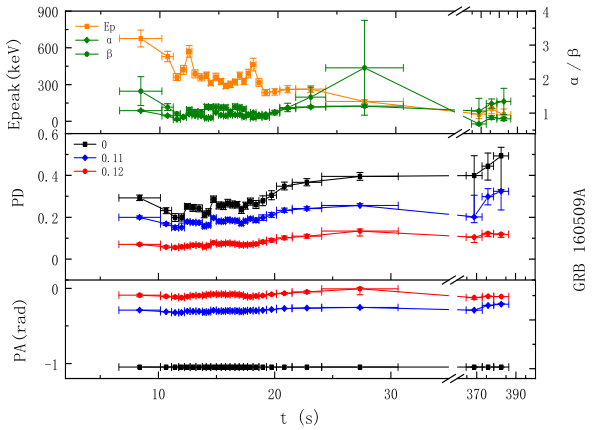


**Figure A4**. Same as Fig. A.1, but for GRB 160509A.

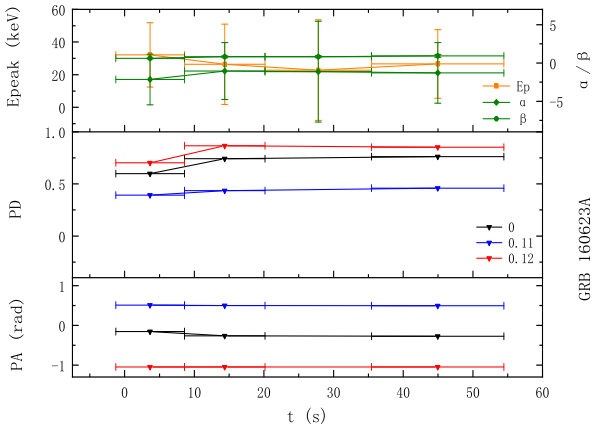


**Figure A5**. Same as Fig. A.1, but for GRB 160623A.

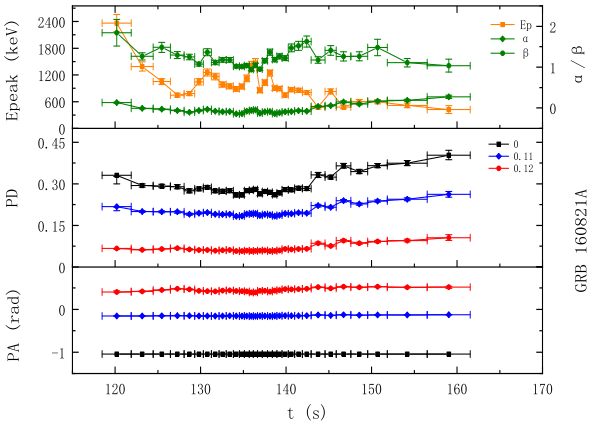


**Figure A6**. Same as Fig. A.1, but for GRB 160821A.

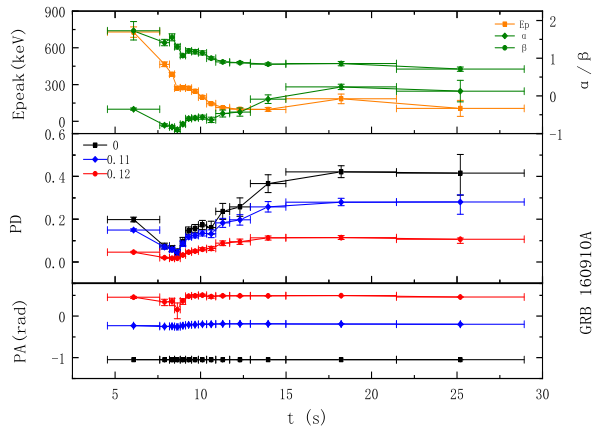


**Figure A7**. Same as Fig. A.1, but for GRB 160910A.

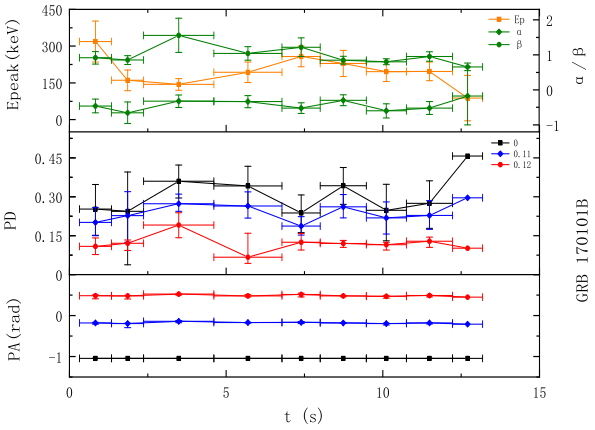


**Figure A8**. Same as Fig. A.1, but for GRB 170101B.

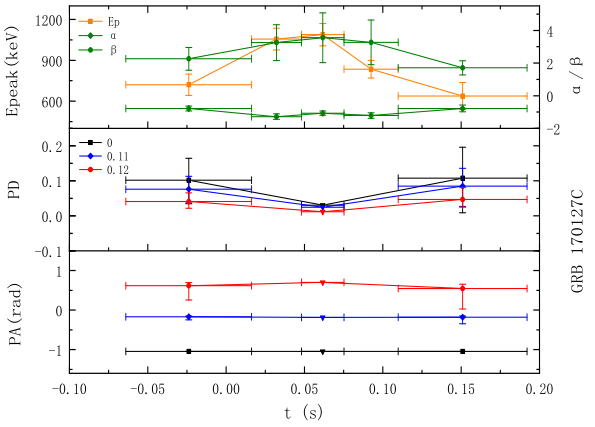


**Figure A9**. Same as Fig. A.1, but for GRB 170127C.

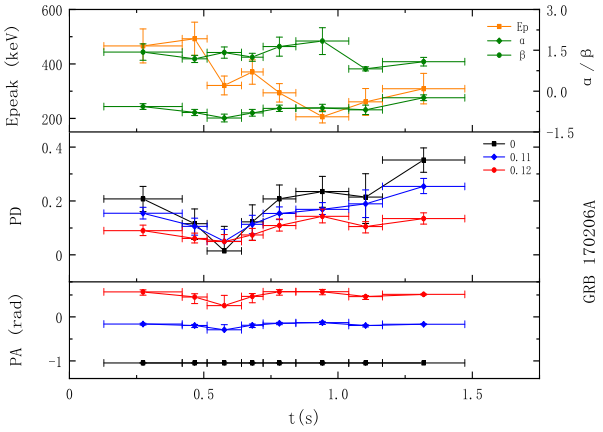


**Figure A10**. Same as Fig. A.1, but for GRB 170206A.

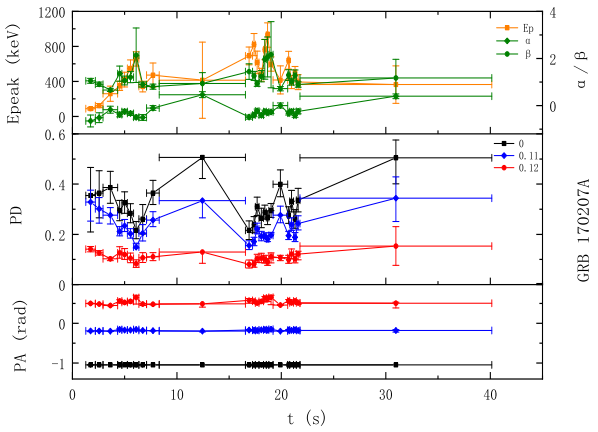


**Figure A11**. Same as Fig. A.1, but for GRB 170207A.

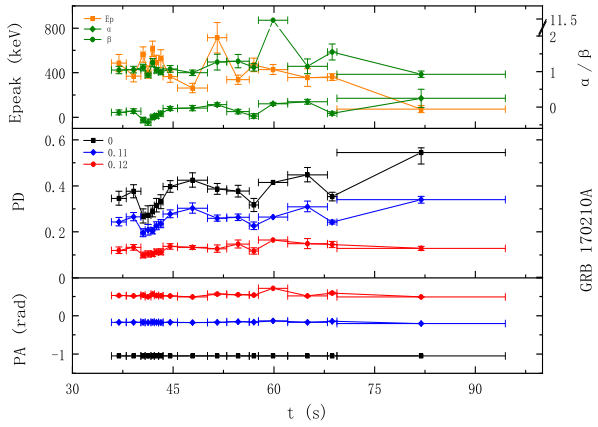


**Figure A12**. Same as Fig. A.1, but for GRB 170210A.

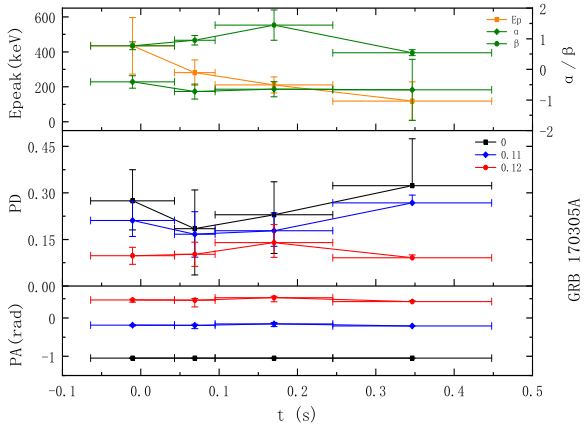


**Figure A13**. Same as Fig. A.1, but for GRB 170305A.

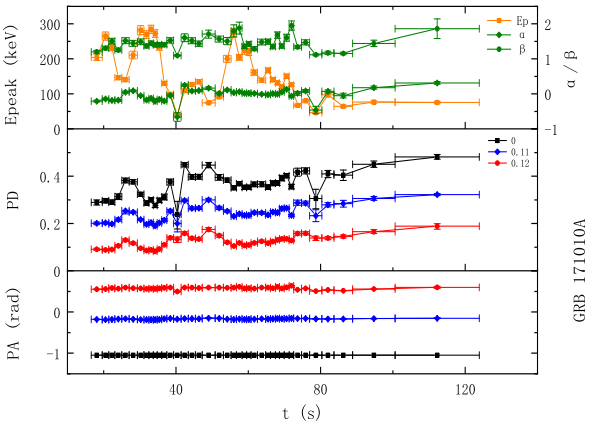


**Figure A14**. Same as Fig. A.1, but for GRB 171010A.

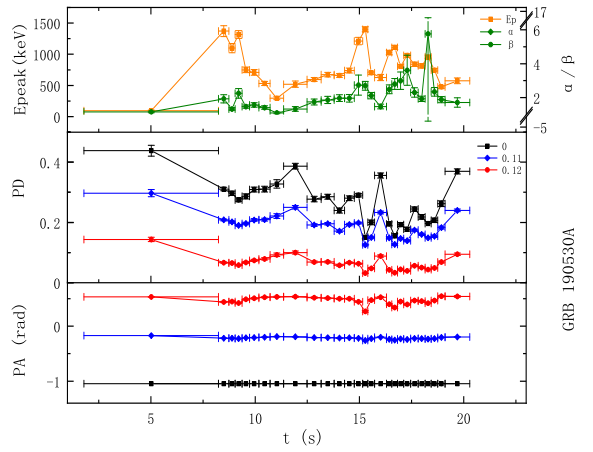


**Figure A15**. Same as Fig. A.1, but for GRB 190530A.